frontiers in Bioengineering and Biotechnology

ORIGINAL RESEARCH
published: 24 September 2021
doi: 10.3389/fbioe.2021.729180

Laminin-1 Peptides Conjugated to Fibrin Hydrogels Promote Salivary Gland Regeneration in Irradiated Mouse Submandibular Glands

*Kihoon Nam[1,2], Harim T. dos Santos[1,2], Frank Maslow[1,2], Bryan G. Trump[3], Pedro Lei[4], Stelios T. Andreadis[4,5,6,7] and Olga J. Baker[1,2,8]**

[1]Bond Life Sciences Center, University of Missouri, Columbia, MO, United States, [2]Department of Otolaryngology-Head and Neck Surgery, School of Medicine, University of Missouri, Columbia, MO, United States, [3]School of Dentistry, University of Utah, Salt Lake City, UT, United States, [4]Department of Chemical and Biological Engineering, University at Buffalo, The State University of New York, Buffalo, NY, United States, [5]Department of Biomedical Engineering, University at Buffalo, The State University of New York, Buffalo, NY, United States, [6]Center of Bioinformatics and Life Sciences, University at Buffalo, The State University of New York, Buffalo, NY, United States, [7]Center of Cell, Gene and Tissue Engineering, University at Buffalo, The State University of New York, Buffalo, NY, United States, [8]Department of Biochemistry, University of Missouri, Columbia, MO, United States

OPEN ACCESS

Edited by:
Carl Austin Gregory, Texas A&M Health Science Center, United States

Reviewed by:
Fei Liu, Texas A&M University, United States
Menekse Ermis Sen, Middle East Technical University, Turkey

***Correspondence:**
Olga J. Baker
bakero@health.missouri.edu

Specialty section:
This article was submitted to Tissue Engineering and Regenerative Medicine, a section of the journal Frontiers in Bioengineering and Biotechnology

Received: *22 June 2021*
Accepted: *23 August 2021*
Published: *24 September 2021*

Citation:
Nam K, dos Santos HT, Maslow F, Trump BG, Lei P, Andreadis ST and Baker OJ (2021) Laminin-1 Peptides Conjugated to Fibrin Hydrogels Promote Salivary Gland Regeneration in Irradiated Mouse Submandibular Glands. Front. Bioeng. Biotechnol. 9:729180. doi: 10.3389/fbioe.2021.729180

Previous studies demonstrated that salivary gland morphogenesis and differentiation are enhanced by modification of fibrin hydrogels chemically conjugated to Laminin-1 peptides. Specifically, Laminin-1 peptides (A99: CGGALRGDN-amide and YIGSR: CGGADPGYIGSRGAA-amide) chemically conjugated to fibrin promoted formation of newly organized salivary epithelium both *in vitro* (*e.g.,* using organoids) and *in vivo* (*e.g.,* in a wounded mouse model). While these studies were successful, the model's usefulness for inducing regenerative patterns after radiation therapy remains unknown. Therefore, the goal of the current study was to determine whether transdermal injection with the Laminin-1 peptides A99 and YIGSR chemically conjugated to fibrin hydrogels promotes tissue regeneration in irradiated salivary glands. Results indicate that A99 and YIGSR chemically conjugated to fibrin hydrogels promote formation of functional salivary tissue when transdermally injected to irradiated salivary glands. In contrast, when left untreated, irradiated salivary glands display a loss in structure and functionality. Together, these studies indicate that fibrin hydrogel-based implantable scaffolds containing Laminin-1 peptides promote secretory function of irradiated salivary glands.

Keywords: biomaterial, hydrogel, regeneration, tissue engineering, saliva, irradiated salivary glands

INTRODUCTION

According to the American Cancer Society, each year more than 80,000 people develop head and neck cancer in the United States (Siegel et al., 2021). A first-line treatment for head and neck cancer is radiation therapy (Sroussi et al., 2017), but ionizing radiation typically leads to chronic oral complications such as xerostomia (i.e., hyposalivation) (Chambers et al., 2004; Grundmann et al., 2010; Jensen et al., 2010; Pinna et al., 2015; Sroussi et al., 2017; Jensen et al., 2019; Haderlein et al., 2020; Jasmer et al., 2020). This condition contributes to oral microbial infections and impairs activities of daily life such as speaking, chewing, and swallowing (Lovelace et al., 2014; Brook, 2021). Existing treatments for hyposalivation are limited to the use

of muscarinic receptor agonists (e.g., cevimeline and pilocarpine) (Braga et al., 2009; Turner, 2016) that induce saliva secretion from the few remaining acinar cells as well as use of saliva substitutes (Silvestre et al., 2009; Rocchi and Emmerson, 2020); however, these therapies target surface-level symptoms and provide only temporary relief (Jaguar et al., 2017; Jensen et al., 2019; Lung et al., 2021). Therefore, development of alternative treatments to restore salivary gland secretory function is critical. Several experimental therapies including the use of stem cells (Nanduri et al., 2011; Nanduri et al., 2013; Pringle et al., 2013; Mitroulia et al., 2019; Su et al., 2020), embryonic organ culture (Ogawa et al., 2013; Ogawa and Tsuji, 2015; Ikeda et al., 2019), organ bioprinting (Ferreira et al., 2016; Adine et al., 2018), cell sheets (Nam et al., 2019a; dos Santos et al., 2020), gene therapy (Zheng et al., 2011; Baum et al., 2012; Arany et al., 2013) and bioengineered scaffolds (Peters et al., 2014; Foraida et al., 2017; Patil and Nanduri, 2017; Nam et al., 2019b) have offered the promise of more advanced solutions as detailed below.

Regarding stem cells/progenitors, previous studies showed that c-Kit$^+$ cells, which normally are found in very low numbers within salivary gland specimens (Nanduri et al., 2011; Nanduri et al., 2013) can be expanded *ex vivo* for restoring salivary gland function; however, further characterization (e.g., how they incorporate into host tissue as well as long term secondary effects such as tumorigenesis and survival rates) must be determined before translating this approach into humans. Another technology involves the use of embryonic organ culture transplantation, where embryonic salivary cells grown in culture can be transplanted *in vivo* (Ogawa et al., 2013); nonetheless, a diminished gland size and an absence of studies showing long-term outcomes following treatment significantly decrease the utility of this model for translational applications. Bioprinting strategies have shown the possibility of assembling glandular compartments (e.g., acinar/ductal epithelial, myoepithelial, endothelial, and neuronal) into salivary gland organotypic cultures; however, this technology does not mimic the salivary gland native architecture (e.g., cell polarity and organization (Ferreira et al., 2016; Adine et al., 2018)). Cell sheets made of salivary gland cells have demonstrated positive results, as they promote cell differentiation and tissue integrity in wounded mouse submandibular gland (SMG) models, yet the main challenge facing this technology is the need to standardize cell composition within the sheets and thereby achieve greater reproducibility (Nam et al., 2019a; dos Santos et al., 2020). Regarding scaffolds other than the Fibrin Hydrogels (FH), various biomaterials (Aframian et al., 2000; Sun et al., 2006; Cantara et al., 2012; Soscia et al., 2013; Hsiao and Yang, 2015; Yang and Hsiao, 2015) have been shown to promote cell growth and attachment but the degree of structural organization, as demonstrated by hollow multi-lumen formation, cell polarity and functionality, has been modest. Likewise, studies have shown that human cells grown on a hyaluronic acid-based scaffold and transplanted into a wounded mouse parotid gland lead to improved secretory function (Pradhan-Bhatt et al., 2014); nevertheless, these results included neither monitoring for degradation of the scaffold nor evidence of new tissue formation, thus raising concerns with the stability of the biomaterial and capacity for regeneration, respectively. Together, these technologies offer the potential for more advanced solutions to hyposalivation due to head and neck radiation therapy but have yet to truly deliver.

In response to these needs and challenges, we developed FH with conjugated Laminin-1 peptides (L_{1p}) A99 and YIGSR that were used successfully to repair salivary gland tissue in a wounded SMG mouse model (Nam et al., 2017a; Nam et al., 2017b; Nam et al., 2019b). To apply these results to a more translational setting, the goal of the current study is to determine whether transdermal injection with the L_{1p} A99 and YIGSR chemically conjugated to FH can promote secretory function in irradiated salivary glands.

MATERIALS AND METHODS

Materials

Lyophilized human fibrinogen, tris base, ethylenediaminetetraacetic acid (EDTA), pilocarpine, isoproterenol, goat serum, hydrochloric acid, hematoxylin, eosin Y solution, Tween® 20, calcium chloride ($CaCl_2$) and ε-aminocaproic acid (εACA) were purchased from MilliporeSigma (Burlington, MA). Rabbit anti-zonula occludens 1 (ZO-1) antibody, rabbit anti-induced nitric oxide synthase (iNOS) antibody, Alexa Fluor 488 conjugated anti-rabbit IgG secondary antibody, Alexa Fluor 568 conjugated anti-rabbit IgG secondary antibody and Alexa Fluor 568 conjugated anti-mouse IgG secondary antibody were purchased from Invitrogen (Carlsbad, CA). Rabbit anti-transmembrane Protein 16A (TMEM16A) antibody and mouse anti-intercellular adhesion molecule (ICAM-1) antibody were purchased from Abcam (Cambridge, MA). Rabbit anti-vascular cell adhesion molecule 1 (VCAM-1) antibody and rabbit Arginase-1 (Arg-1) antibody were purchased from Cell Signaling Technology (Danvers, MA). Mouse anti-Na^+/K^+-ATPase antibody was purchased from Santa Cruz Biotechnology (Dallas, TX). Mouse anti-E-cadherin antibody was purchased from BD Biosciences (San Jose, CA). Phosphate buffered saline (PBS), DyLight™ 680 NHS-ester, 4′,6-diamidino-2-phenylindole (DAPI), Triton X-100, sodium citrate, xylene and ethanol were purchased from Thermo Fisher Scientific (Waltham, MA). Ketamine and xylazine were purchased from VetOne (Boise, ID). Insulin syringes (28G) were purchased from BD (Franklin Lakes, NJ). Peptides were synthesized by University of Utah DNA/Peptide synthesis core facility, as previously described (Nam et al., 2016; Nam et al., 2017a; Nam et al., 2017b).

Animals

Female 6-week-old C57BL/6J mice weighing ~17–20 g were purchased from Jackson Laboratory (Bar Harbor, ME). Power analysis was performed to determine mouse numbers using G*Power 3.1.9.7 software (Heinrich-Heine-Universität Düsseldorf, Düsseldorf, Germany; http://www.gpower.hhu.de/). All calculations were conducted using a significance level of 0.05 with 95% power. Then, 105 mice were randomly distributed into

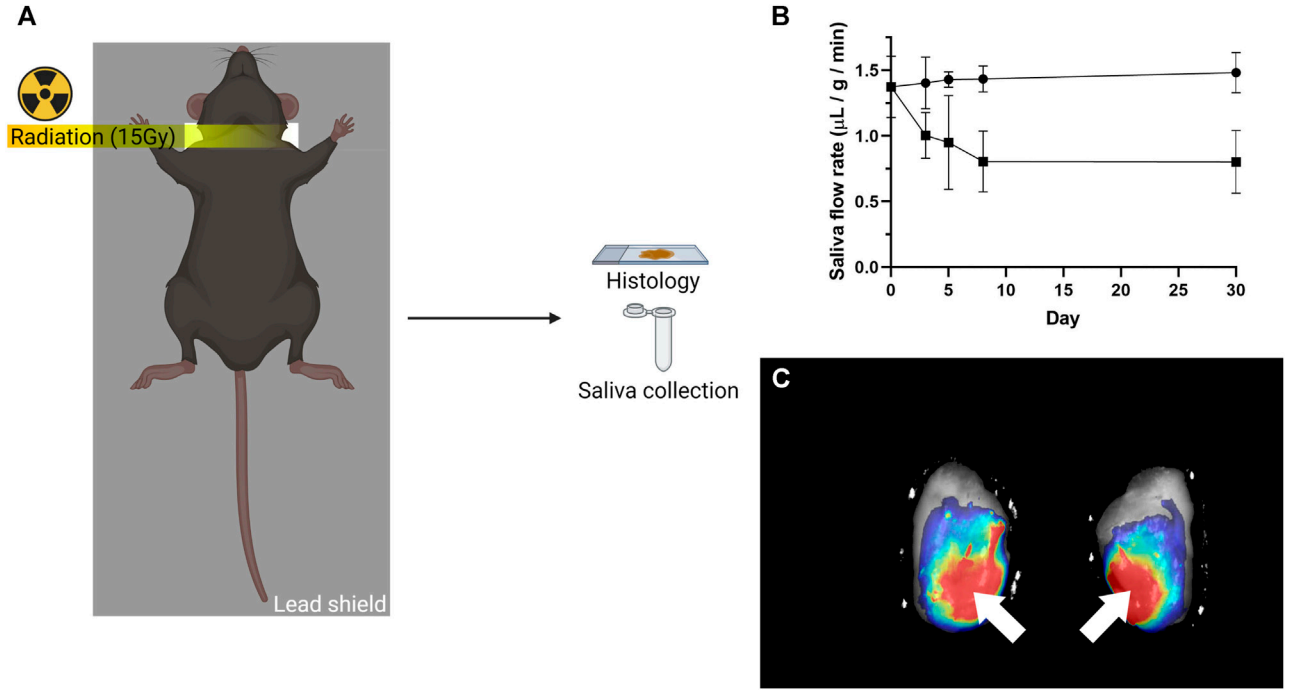

FIGURE 1 | Radiation treatment and local L_{1P}-FH delivery used in this study. **(A)** Mice received a single 15 Gy radiation dose with a customized lead shield having a 1 cm slit aligned to the mouse's neck. **(B)** Radiation treatment caused saliva flow rates to be significantly reduced. The symbol (●) indicates non-irradiated group, while the symbol (■) indicates irradiated group. **(C)** DyLight 680 conjugated L_{1P}-FH were successfully delivered to the mouse submandibular glands when applied via transdermal injection. White arrows indicate the site of L_{1p}-FH injection.

three groups to receive the following treatments: non-irradiated (40 mice), irradiated without L_{1p}-FH injection (40 mice), and irradiated while also receiving the L_{1p}-FH injection (25 mice), comprising treatment groups 1–3, respectively. All animal usage, anesthesia and surgeries were conducted with the approval of the University of Utah Institutional Animal Care and Use Committee (IACUC) in compliance with the ARRIVE guidelines.

Radiation Treatment

Salivary gland tissue damage is a late degenerative response observed after radiation therapy (Wu and Leung, 2019; Jasmer et al., 2020). To confirm L_{1p}-FH regenerative effects in a more clinically relevant animal model, a widely accepted head and neck irradiated mouse model was used for this study (Deasy et al., 2010; Varghese et al., 2018). Briefly, mice were anesthetized with ketamine (100 mg/kg) and xylazine (5 mg/kg) solution administered intraperitoneally with the head and neck area positioned over the 1 cm slit of a customized lead shield, thereby protecting other areas of the body from radiation. SMGs then received a single 15 Gy radiation dose using a JL Shepherd ^{137}Cs irradiator (**Figure 1A**). Animals were allowed to recover for 3 days and received hydrogel treatment soon after, as detailed below.

Hydrogel Preparation

Peptides and DyLight 680 conjugated fibrinogen were prepared, as previously described (Nam et al., 2017a; Nam et al., 2017b). Briefly, two Laminin-1 peptides (A99 and YIGSR) were synthesized on a peptide synthesizer. Peptides were then conjugated to the fibrinogen using sulfo-LC-SPDP and cysteine residue in peptides. In addition, fibrinogen was chemically labeled with a fluorescent dye through NHS ester of DyLight 680. Finally, laminin-1 peptide conjugated fibrinogens and DyLight 680 labeled fibrinogen were dialyzed against ultrapure water, lyophilized, and stored at −80°C until use. L_{1p}-FH were prepared similar to previous studies (Nam et al., 2017a; Nam et al., 2017b) except for the use of exogenous thrombin (thereby preventing rapid polymerization inside the syringe) as follows: YIGSR-conjugated fibrinogen (1.2 mg/ml), A99-conjugated fibrinogen (1.2 mg/ml), DyLight 680 conjugated fibrinogen (0.1 mg/ml), $CaCl_2$ (2.5 mM) and εACA (2 mg/ml) were mixed in a tris buffered saline (TBS) solution. Polymerization of L_{1p}-FH was confirmed from fluorescence in the SMG of randomly selected mice (**Figure 1C**).

Transdermal Injection

C57BL/6J mice were anesthetized with 3% isoflurane using an oxygen flow rate set at 2.0 L/min, and 10 µL of freshly mixed L_{1p}-FH solution was transdermally injected using insulin syringe (G 28) to irradiated mouse SMGs at post-radiation day 3. L_{1p}-FH effects were studied at days 8 and 30. Using thrombin prior transdermal injection causes rapid polymerization of L_{1p}-FH which clogs the needle. To overcome this issue, the mixture was applied in a liquid form using endogenous thrombin for internal polymerization. To confirm scaffold implantation *in*

vivo, FH was labeled with DyLight 680 and quantified within dissected glands using a Bio-Rad Chemi-Doc™ MP imaging system (**Figure 1C**).

Hematoxylin and Eosin and Masson's Trichrome Stain

SMGs were fixed in 10% formalin at room temperature overnight, dehydrated in 70% ethanol solution, embedded in paraffin wax and cut into 3 μm sections. Sections were then deparaffinized with xylene and rehydrated with serial ethanol solutions (100%, 95% 80, 70 and 50%, v/v) and distilled water. For hematoxylin and eosin staining, the rehydrated sections were stained with hematoxylin for 5 min, washed with distilled water for 5 min, tap water for 5 min and distilled water for 2 min. Next, slides were stained with eosin for 30 s, washed with tap water for 5 min and distilled water for 2 min. Finally, hematoxylin and eosin stained gland sections were dehydrated with 95 and 100% ethanol (v/v), cleared in xylene and mounted with a xylene-based mounting medium. As for Masson's trichrome staining, the rehydrated sections were re-fixed in Bouin's solution at 60°C for 1 h then washed with running tap water for 10 min and distilled water for 5 min. Next, sections were stained with Weigert's iron hematoxylin solution for 10 min then washed with running warm tap water for 10 min and distilled water for 5 min. For cytoplasm staining, sections were incubated with Biebrich scarlet acid fuchsine solution for 5 min and washed three times with distilled water for 2 min. Regarding collagen staining, sections were incubated in phosphotungstic/phosphomolybdic acid for 15 min, stained with aniline blue solution for 5 min and washed three times with distilled water for 2 min. Stained sections were then differentiated in 1% acetic acid solution for 1 min and washed two times with distilled water for 2 min. Finally, Masson's trichrome stained sections were dehydrated with serial ethanol solutions (95 and 100%), cleared in xylene and mounted with a xylene-based mounting medium. Finally, the samples were analyzed using a Leica DMI6000B (Leica Microsystems, Wetzlar, Germany) to determine tissue morphology.

Confocal Analysis

For antigen retrieval, the rehydrated and fixed tissue sections were incubated in Tris-EDTA buffer [10 mM Tris, 1 mM EDTA, 0.05% (v/v) Tween® 20, pH 9.0] for ZO-1 and E-cadherin or with sodium citrate buffer [10 mM sodium citrate, 0.05% (v/v) Tween® 20, pH 6.0] for TMEM16A, Na^+/K^+-ATPase, iNOS, Arg-1, VCAM-1 and ICAM-1 at 95°C for 30 min. Next, samples were permeabilized with 0.1% (v/v) triton X-100 in PBS at room temperature for 45 min. Specimens were then blocked in 5% (v/v) goat serum in PBS for 1 h at room temperature and incubated at 4°C with the following primary antibodies overnight: rabbit anti-ZO-1, mouse anti-E-cadherin, rabbit anti-TMEM16A, mouse anti-Na^+/K^+-ATPase, rabbit anti-VCAM-1 or mouse anti-ICAM-1. At that time, sections were incubated with anti-rabbit Alexa Fluor 488 and anti-mouse Alexa Fluor 568 secondary antibodies in 5% goat serum at room temperature for 1 h followed by 300 nM DAPI staining at room temperature for 5 min. For M1 and M2 marker staining, specimens were blocked in 3% (w/v) bovine serum albumin (BSA) in PBS for 1 h at room temperature and incubated with primary antibodies (rabbit anti-iNOS or rabbit anti-Arg-1) at 37°C for 1 h. Then, sections were incubated with anti-rabbit Alexa Fluor 568 in 3% BSA at room temperature for 1 h followed by 300 nM DAPI staining at room temperature for 5 min. Finally, specimens were analyzed using a STELLARIS Confocal Microscope (Leica Microsystems, Wetzlar, Germany).

Macrophage Ratio

M1 and M2 macrophage cells were determined using ImageJ. Specifically, the color threshold was set to isolate the colocalized signal of nuclei and M1 (**Figure 4**, white arrows)/M2 (**Figure 4**, red arrows) positive cells, which were counted and normalized by area. Statistical significance was assessed using one-way ANOVA ($^*p < 0.01$) and Dunnett's post-hoc test for multiple comparisons to group 2 (irradiated with no L_{1p}-FH injection at day 30).

Saliva Flow Rate Measurements

Mice were anesthetized with ketamine (100 mg/kg) and xylazine (5 mg/kg) followed by intraperitoneal injection with pilocarpine (25 mg/kg) and isoproterenol (0.5 mg/kg). Then, whole saliva was collected using a micropipette for 5 min and flow rate was calculated using the following formula:

$$\text{Saliva flow rate} = \frac{\text{Stimulated saliva } (\mu L)}{\text{Body weight of mouse } (g) \text{ x collection time } (5 min)}$$

Statistical Analysis

Experimental data were analyzed using one-way ANOVA and Dunnett's post hoc test for multiple comparisons to the non-irradiated group 1 at day 30. All values represent means ± SD ($n = 5$), where p values <0.01 were considered statistically significant. Finally, these calculations were performed using GraphPad Prism 6.

RESULTS

A Head and Neck Irradiated Mouse Model was Achieved

To investigate whether L_{1p}-FH could restore irradiated SMG structure and function, C57BL/6J mice were subjected to a single radiation treatment as described in Materials and Methods (**Figure 1A**). Mice treated with a single 15 Gy radiation dose displayed a significant reduction in saliva flow rates as compared to non-irradiated controls (i.e., from 1.43 to 0.80 μL/g/min, $n = 5$, $p < 0.01$) in the first 8 days and remained steady thereafter until day 30 (**Figure 1B**). These results demonstrated that the radiation dose utilized here caused significant loss of salivary secretory function and can thus be used as a head and neck irradiated preclinical model, consistent with previous studies (Lombaert et al., 2008; Varghese et al., 2018; Weng et al., 2018).

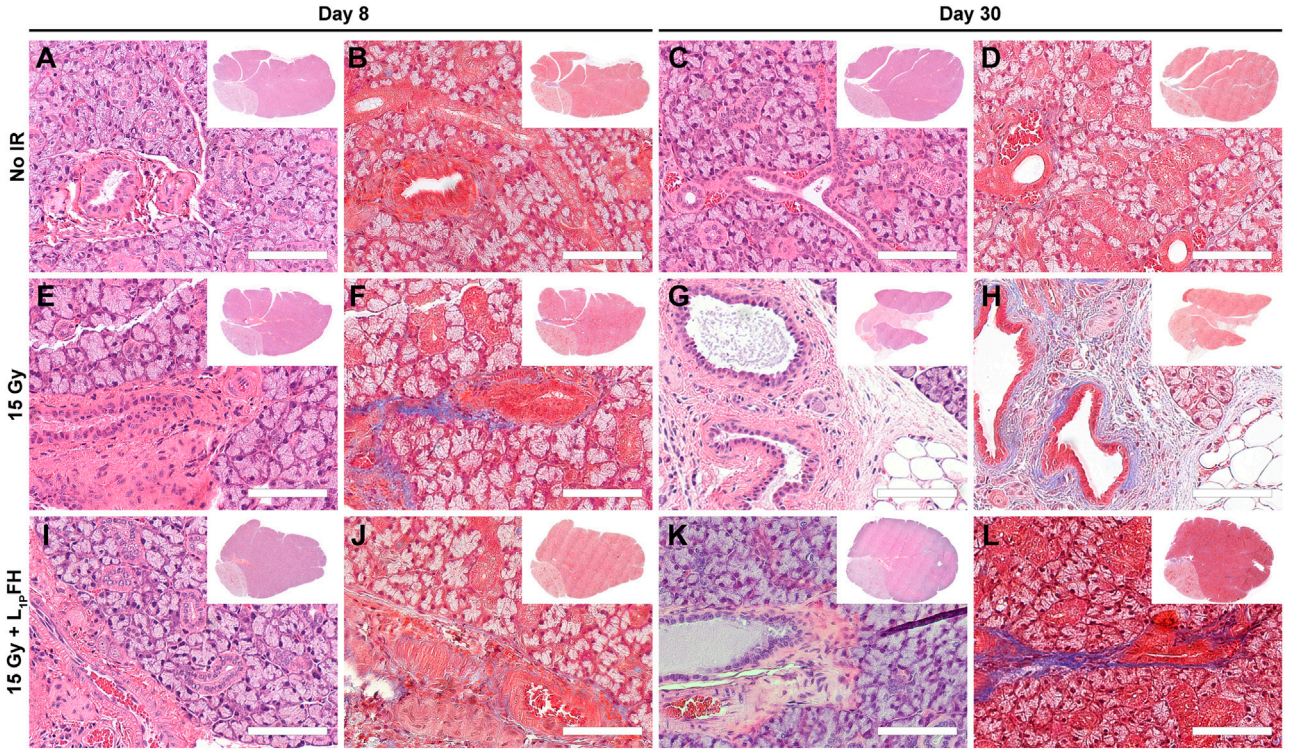

FIGURE 2 | Treatment with L_{1p}-FH preserves epithelial integrity when applied after radiation treatment. Hematoxylin and eosin **(A,C,E,G,I,K)** as well Masson's trichrome **(B,D,F,H,J,L)** staining of mouse submandibular glands from group 1 [non-irradiated, **(A–D)**], group 2 [irradiated without L_{1p}-FH injection, **(E–H)**] and group 3 [irradiated with L_{1p}-FH injection, **(I–L)**] were performed and tissue morphology was analyzed using a Leica DMI6000B. Scale bars represent 100 μm. Representative image from a total of five mice per group.

L_{1p}-FH was Successfully Implanted in Irradiated Mouse Submandibular Glands

Our previous studies showed the biocompatibility of L_{1p}-FH with host tissue when surgically implanted in a wounded mouse model (Nam et al., 2017a; Nam et al., 2017b). To avoid an open wound surgery, we attempted to deliver the L_{1p}-FH to irradiated mouse SMG via transdermal injection as described in Materials and Methods. For these experiments, we used a fluorescently labeled hydrogel using DyLight 680 and successfully implanted L_{1p}-FH in irradiated mouse SMG *via* transdermal injection (**Figure 1C**, white arrows).

L_{1p}-FH Preserved Epithelial Integrity After Radiation Treatment

Our previous studies showed that L_{1p}-FH promoted tissue repair in a wounded SMG mouse model (Nam et al., 2017a; Nam et al., 2017b; Nam et al., 2019b). To determine whether these effects occur in the head and neck irradiated mouse model, we randomly distributed mice in three groups and applied this scaffold as follows: non-irradiated, irradiated without L_{1p}-FH injection and irradiated that received the L_{1p}-FH injection, comprising treatment groups 1–3, respectively (see Material and Methods section). As shown in **Figure 2**, group 1 (non-irradiated glands) displayed intact lobules where the parenchyma was separated by areas of thin connective tissue at days 8 (**Figures 2A,B**) and 30 (**Figures 2C,D**). As for cytologic features, serous acini cells showed a typical pyramidal shape with basophilic cytoplasm and basal nuclei. In contrast, mucous cells showed a pale cytoplasm with flat basilar nuclei, intercalated ducts were lined by cuboidal and/or flat cells, striated ducts showed cuboidal to low columnar cells and granular convoluted ducts were lined by tall columnar cells containing intracytoplasmic eosinophilic granules. Together, these features indicate that the non-irradiated glands in group 1 showed the morphology of a healthy epithelium. In contrast, group 2 (irradiated with no L_{1p}-FH injection) demonstrated glandular parenchyma separated by thicker connective tissue strands, ductal areas with ectasia, intraluminal depositions and increased presence of fibrosis when compared to controls (**Figures 2E,F**). Furthermore, tissue damage was even more severe at day 30 (**Figures 2G,H**), where SMG showed an extensive disruption of the lobular architecture as indicated by the replacement of acini and ducts with sheets of vacuolated cells, adipocytes and fibrosis. Together, these results indicated that irradiated glands with no L_{1p}-FH injection (group 2) dramatically lost epithelial integrity. Remarkably, mice in group 3 (irradiated with L_{1p}-FH injection) recovered many of the features of healthy glands. For instance, we observed the presence of serous acinar units with organized ductal structures surrounded by thin connective tissue strands

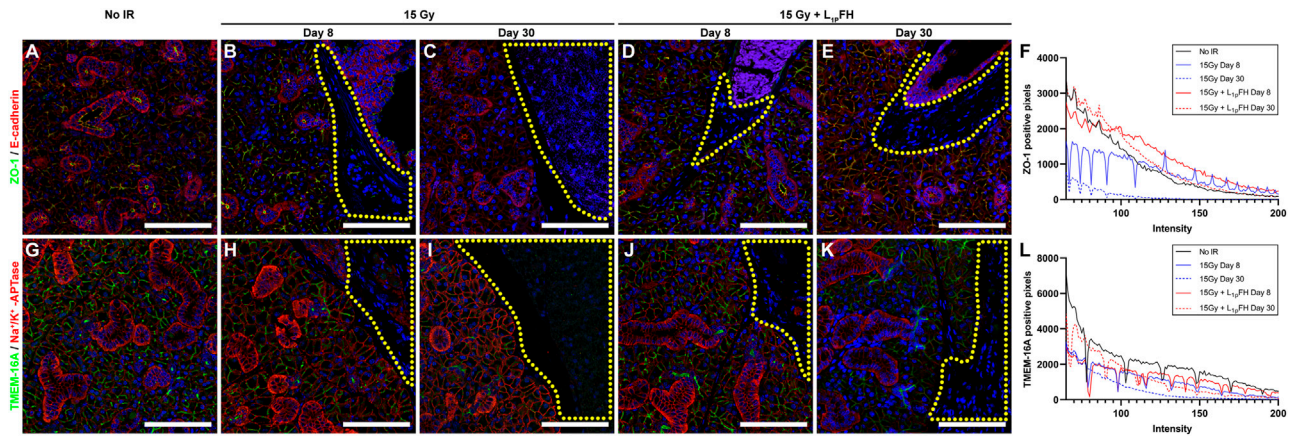

FIGURE 3 | Treatment with L_{1p}-FH maintains epithelial polarity and functional marker expression. Salivary structural and functional marker organization was analyzed using confocal microscopy with specific antibodies against ZO-1 [green; **(A–E)**], E-cadherin [red; **(A–E)**], TMEM16A [green; **(G–K)**], Na^+/K^+-ATPase [red; **(G–K)**], and DAPI (blue; everywhere). Scale bars represent 100 μm. Yellow-dotted areas indicate fibroblast-like areas. Representative image from a total of five mice per group. ZO-1 **(F)** and TMEM-16A **(L)** positive pixels were analyzed using ImageJ.

similar to the non-irradiated group 1 at both days 8 (**Figures 2I,J**) and 30 (**Figures 2K,L**). These changes indicate that group 3 (irradiated glands treated with L_{1p}-FH) had a morphology consistent with a healthy salivary gland epithelium and results in this section indicate that L_{1p}-FH is a suitable scaffold for promoting epithelial integrity in irradiated SMG.

L_{1p}-FH Maintained Epithelial Polarity and Preserved Ion Transporter Expression

To determine whether L_{1p}-FH maintained epithelial polarity in an irradiated mouse model, we stained the SMG sections with the apical tight junction marker ZO-1 and basolateral marker E-cadherin. As shown in **Figure 3A**, group 1 (non-irradiated glands) displayed apical ZO-1 (green) and basolateral E-cadherin (red) after 30 days. However, in group 2 (irradiated glands with no L_{1p}-FH injection), a mild residual ZO-1 signal was detected at day 8 (**Figures 3B,F**, blue solid line), and a weaker ZO-1 signal was expressed at day 30 (**Figure 3F**, blue dotted line), together with ZO-1 disorganization (**Figure 3C**), thereby indicating loss of epithelial polarity. In contrast, group 3 (irradiated glands treated with L_{1p}-FH) showed apical ZO-1 and basolateral E-cadherin signals both at days 8 (**Figure 3D**) and 30 (**Figure 3E**), indicating that the scaffold treatment helps to maintain epithelial polarity (**Figure 3F**, red line and red dotted line). Regarding the presence of functional markers, group 1 (non-irradiated SMG) showed apical TMEM16A (**Figure 3G**, green) and basolateral Na^+/K^+-ATPase localization (**Figure 3G**, red) at day 30, consistent with a healthy salivary epithelium. In contrast, group 2 (irradiated glands with no L_{1p}-FH injection) showed a moderate TMEM16A signal (**Figure 3L**, blue solid line) at day 8 (**Figure 3H**, green) and weaker TMEM16A signal (**Figure 3L**, blue dotted line) at day 30 (**Figure 3I**, green). Interestingly, group 3 (irradiated glands treated with L_{1p}-FH) expressed strong apical TMEM16 (**Figures 3J,K**, green; **Figure 3L**, red line and red dotted line) and basolateral Na^+/K^+-ATPase similar to non-irradiated glands, thus suggesting that L_{1p}-FH treatment helps to maintain epithelial polarity and preserve ion transport expression, both of which are critical for saliva secretion.

L_{1p}-FH Promoted Macrophage Polarization

Our previous studies indicated that treatment with L_{1p}-FH promoted macrophage polarization in a wounded SMG female mouse model (Brown et al., 2020). To determine whether similar effects occur in an irradiated mouse model, we identified the presence of M1 and M2 subtypes within the SMG using macrophage-specific antibodies (i.e., iNOS and Arg-1, corresponding to M1 and M2, respectively). As shown in **Figures 4A,F**, group 1 (non-irradiated glands) expressed iNOS-positive cells with approximately 0.94 macrophages per 100,000 μm (Sroussi et al., 2017). In contrast, group 2 (irradiated glands with no L_{1p}-FH injection) showed a significant increase in M1 macrophages (approximately 28.65 iNOS-positive cells) at day 30 (**Figures 4C,F**). Notably, group 3 (irradiated glands treated with L_{1p}-FH) showed a significant decrease of M1 macrophages (approximately 5.92 iNOS-positive cells) at day 30 (**Figures 4E,F**) compared to group 2. Regarding the presence of M2 markers, group 2 (irradiated glands with no L_{1p}-FH injection) expressed Arg-1-positive cells with approximately 5.92 macrophages at day 30 (**Figures 2I,L**), which is not a significant difference from group 1 (**Figures 4G,L**, 2.60 macrophages). Interestingly, group 3 (irradiated glands treated with L_{1p}-FH) expressed a significant increase of Arg-1-positive cells at day 30 (approximately 11.37 macrophages, **Figure 4K,L**). Together, these results indicate that L_{1p}-FH causes a decrease in M1 macrophages together with an increase in M2 macrophages in SMG following radiation treatment.

L_{1p}-FH Increased Saliva Secretion After Radiation Treatment

Our previous studies indicate that treatment with L_{1p}-FH enhances saliva secretion in a wounded SMG mouse model

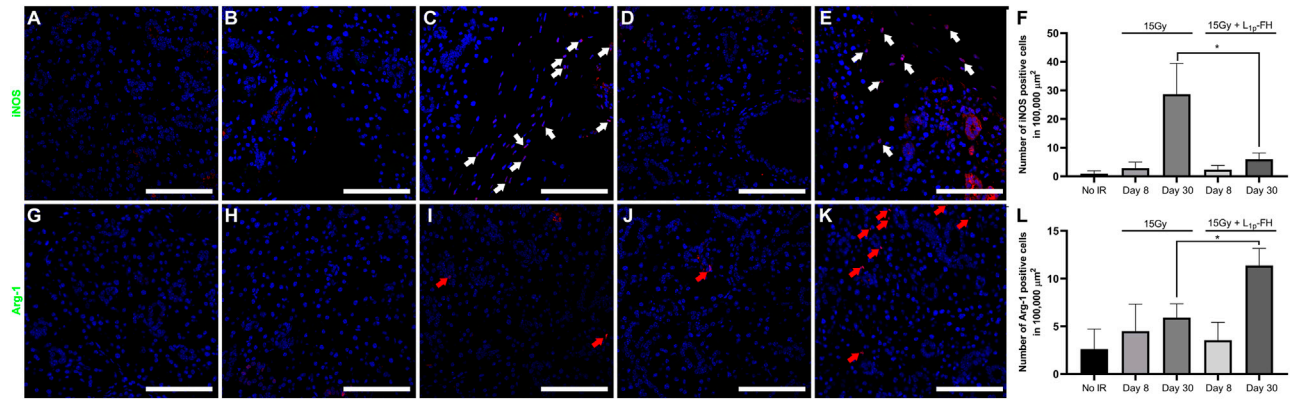

FIGURE 4 | L_{1p}-FH promotes macrophage polarization. Macrophage marker expression was analyzed using confocal microscopy with specific antibodies against iNOS **(A–F)**, Arg-1 **(G–L)**, and DAPI (blue; everywhere). Scale bars represent 100 μm. White and red arrows indicate iNOS or Arg-1 positive cells, respectively. Representative image from a total of five mice per group. iNOS **(F)** and Arg-1 **(L)** positive cells were analyzed using ImageJ and GraphPad Prism 6. Data represent the means ± SD of $n = 5$ mice per condition with statistical significance assessed using one-way ANOVA (*$p < 0.01$) and Dunnett's post-hoc test for multiple comparisons to group 2 (irradiated with no L_{1p}-FH injection at day 30).

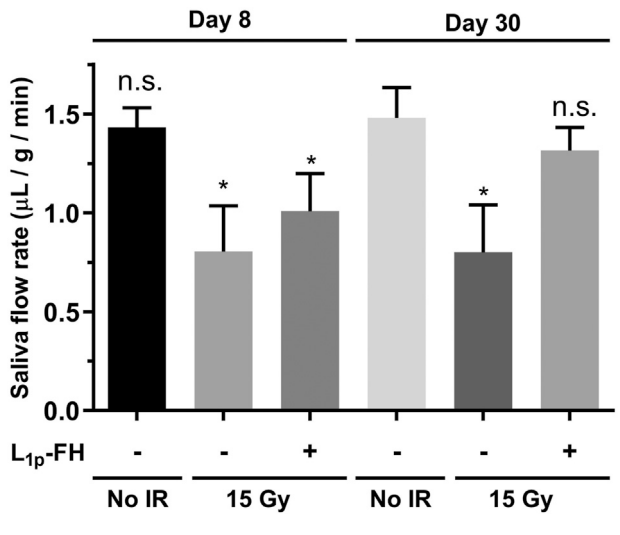

FIGURE 5 | L_{1p}-FH increases saliva secretion after radiation treatment. Mice were anesthetized and stimulated with pilocarpine and isoproterenol at days 8 and 30 with saliva collected for 5 min. Data represent the means ± SD of $n = 5$ mice per condition with statistical significance assessed using one-way ANOVA (*$p < 0.01$) and Dunnett's post-hoc test for multiple comparisons to group 1 (non-irradiated mice at day 30). The symbol (+) indicates L_{1p}-FH injection, while the symbol (–) indicates no L_{1p}-FH injection, and n. s indicates no significant differences from group 1 (non-irradiated mice at day 30).

(Nam et al., 2017a; Nam et al., 2017b; Nam et al., 2019b). To determine whether similar effects occur in an irradiated mouse model, we treated irradiated SMG with a transdermal injection of L_{1p}-FH as described in Materials and Methods. As shown in **Figure 5**, group 1 (non-irradiated glands) showed intact saliva flow rates (i.e., 1.43 μL/g/min), as expected. In contrast, group 2 (irradiated untreated glands) exhibited a significant reduction in saliva flow rates (i.e., 0.80 μL/g/min, $n = 5$, $p < 0.01$). Notably, group 3 (irradiated glands treated with L_{1p}-FH) showed a significant increase of saliva flow rates (1.32 μL/g/min, $n = 5$, $p < 0.01$) at day 30, thereby demonstrating that L_{1p}-FH restores saliva secretion after radiation treatment.

DISCUSSION

Our previous studies indicated that treatment with FH alone promotes neither cell polarity nor differentiation in salivary gland epithelium, both *in vitro or in vivo* (Nam et al., 2016; Nam et al., 2017a; Nam et al., 2017b; Nam et al., 2019b; Dos Santos et al., 2021). However, specific L_{1p} sequences (A99: CGGALRGDN-amide, YIGSR: CGGADPGYIGSRGAA-amide) proved to be useful for improving salivary gland regeneration (Hoffman et al., 1998). Specifically, freshly isolated SMG cells grown on L_{1p} chemically attached to FH induced lumen formation and secretory function (Nam et al., 2016). Moreover, L_{1p}-FH promoted salivary gland regeneration in an *in vivo* wound-healing mouse model (Nam et al., 2017a; Nam et al., 2017b), thus leading to increased saliva secretion. Such functional recovery indicates that FH-based scaffolds can be used to promote salivary gland function in radiation-induced hyposalivation. Additionally, we developed a transdermal delivery system specifically for this study with the aim of using the patient's own blood for polymerization to increase biocompatibility (Froelich et al., 2010; Dietrich et al., 2013) and having the ancillary benefits of displaying optimal rheological properties (i.e., softness) and being less invasive than other delivery methods (i.e., retro-ductal delivery (Nair et al., 2016) and surgical application (Ogawa et al., 2013)), all of which indicates a greater degree of clinical applicability for our newly designed mouse model.

Regarding results of the current study, salivary gland morphology was significantly improved by L_{1p}-FH

(**Figures 2I–L** and **Figure 3D,E**) and saliva secretion (**Figure 5**) was likewise restored by day 30 post-radiation; however, such treatment gains cannot be counted on to persist, given the residual fibrosis noted (**Figure 2L**). Additionally, future studies will use growth factors specifically targeted for angiogenesis (i.e., VEGF and FGF9) (Nam et al., 2019b) in response to current results demonstrating L_{1p}-FH promoted macrophage polarization (**Figure 4**) but gave rise to no blood vessel formation (**Supplementary Figure S1**). Moreover, should such gains in fact prove persistent (e.g., maintained over long periods of time), we as yet have limited knowledge of the mechanisms responsible for this recovery. These issues notwithstanding, the results to date are important because they are the first time that L_{1p}-FH has been used in irradiated glands to restore their form and function.

It is noteworthy to mention three major differences between our previous studies and the current work. First, our previous studies used L_{1p} in trimeric form (Dos Santos et al., 2021) and in combination with growth factors (Nam et al., 2019b), while the current work employs only monomeric forms and no growth factors. Next, our previous studies used a more invasive SMG surgical punch model (Nam et al., 2017a; Nam et al., 2017b; Nam et al., 2019b) as compared to currently used transdermal injection implantation method. Finally, we replaced the SMG wounded mouse model of our prior studies with a radiation model for greater specificity in terms of clinical features and increased translational application.

To expand on this work, future studies will perform extended saliva secretion studies and track the appearance of fibrosis at multiple time points via histological studies and investigate how L_{1p} used here (i.e., A99 (Mochizuki, 2003; Rebustini et al., 2007; David et al.,2008) and YIGSR (Caiado and Dias, 2012; Frith et al., 2012; Huettner et al., 2018; Motta et al., 2019)) bind to specific integrins, thus addressing the questions noted above in relation to treatment duration and mechanisms. Finally, should this treatment near the stage of clinical trials, it would be important to replace the current single dose of radiation used for proof of concept and early exploration with more clinically appropriate fractionated doses.

DATA AVAILABILITY STATEMENT

The original contributions presented in the study are included in the article/**Supplementary Material**, further inquiries can be directed to the corresponding author.

ETHICS STATEMENT

The animal study was reviewed and approved by University of Utah IACUC.

AUTHOR CONTRIBUTIONS

KN, SA, and OB conceived the idea; KN, HS, and OB designed the study, and wrote the manuscript; KN, HS, FM, and BT performed all the experiments and/or analyzed the data; KN, SA, and OB directed the project; PL, SA, KN, and OB provided technical support, and corrections to the manuscript; KN and OB revised the manuscript according to the comments of all co-authors. All authors reviewed the manuscript and approved the submitted version.

FUNDING

This study is supported by the National Institutes of Health–National Institute of Dental and Craniofacial Research (grant R01DE022971 to OB and SA and grant R01DE027884 to OB).

SUPPLEMENTARY MATERIAL

The Supplementary Material for this article can be found online at: https://www.frontiersin.org/articles/10.3389/fbioe.2021.729180/full#supplementary-material

Supplemental Figure S1 | L_{1p}-FH does not enhance angiogenesis after radiation treatment. VCAM-1 (green) and ICAM-1 (red) were analyzed using confocal microscopy. Scale bars represent 100 μm. Representative image from a total of 5 mice per group.

REFERENCES

Adine, C., Ng, K. K., Rungarunlert, S., Souza, G. R., and Ferreira, J. N. (2018). Engineering Innervated Secretory Epithelial Organoids by Magnetic Three-Dimensional Bioprinting for Stimulating Epithelial Growth in Salivary Glands. *Biomaterials* 180, 52–66. doi:10.1016/j.biomaterials.2018.06.011

Aframian, D. J., Cukierman, E., Nikolovski, J., Mooney, D. J., Yamada, K. M., and Baum, B. J. (2000). The Growth and Morphological Behavior of Salivary Epithelial Cells on Matrix Protein-Coated Biodegradable Substrata. *Tissue Eng.* 6, 209–216. doi:10.1089/10763270050044380

Arany, S., Benoit, D. S., Dewhurst, S., and Ovitt, C. E. (2013). Nanoparticle-mediated Gene Silencing Confers Radioprotection to Salivary Glands *In Vivo*. *Mol. Ther.* 21, 1182–1194. doi:10.1038/mt.2013.42

Baum, B. J., Alevizos, I., Zheng, C., Cotrim, A. P., Liu, S., McCullagh, L., et al. (2012). Early Responses to Adenoviral-Mediated Transfer of the Aquaporin-1 cDNA for Radiation-Induced Salivary Hypofunction. *Proc. Natl. Acad. Sci.* 109, 19403–19407. doi:10.1073/pnas.1210662109

Braga, M., Tarzia, O., Bergamaschi, C., Santos, F., Andrade, E., and Groppo, F. (2009). Comparison of the Effects of Pilocarpine and Cevimeline on Salivary Flow. *Int. J. Dent Hyg.* 7, 126–130. doi:10.1111/j.1601-5037.2008.00326.x

Brook, I. (2021). *Early Side Effects of Radiation Treatment for Head and Neck Cancer*. Cancer/Radiothérapie.

Brown, C. T., Nam, K., Zhang, Y., Qiu, Y., Dean, S. M., Dos Santos, H. T., et al. (2020). Sex-dependent Regeneration Patterns in Mouse Submandibular Glands. *J. Histochem. Cytochem.* 68, 305–318. doi:10.1369/0022155420922948

Caiado, F., and Dias, S. (2012). Endothelial Progenitor Cells and Integrins: Adhesive Needs. *Fibrogenesis Tissue Repair* 5, 4. doi:10.1186/1755-1536-5-4

Cantara, S. I., Soscia, D. A., Sequeira, S. J., Jean-Gilles, R. P., Castracane, J., and Larsen, M. (2012). Selective Functionalization of Nanofiber Scaffolds to Regulate Salivary Gland Epithelial Cell Proliferation and Polarity. *Biomaterials* 33, 8372–8382. doi:10.1016/j.biomaterials.2012.08.021

Chambers, M. S., Garden, A. S., Kies, M. S., and Martin, J. W. (2004). Radiation-induced Xerostomia in Patients with Head and Neck Cancer: Pathogenesis, Impact on Quality of Life, and Management. *Head Neck* 26, 796–807. doi:10.1002/hed.20045

David, R., Shai, E., Aframian, D. J., and Palmon, A. (2008) Isolation and Cultivation of Integrin α6β1–Expressing Salivary Gland Graft Cells: A Model for Use with an Artificial Salivary Gland. *Tissue Eng. A* 14, 331–337. doi:10.1089/tea.2007.0122

Deasy, J. O., Moiseenko, V., Marks, L., Chao, K. S. C., Nam, J., and Eisbruch, A. (2010). Radiotherapy Dose-Volume Effects on Salivary Gland Function. *Int. J. Radiat. Oncology*Biology*Physics* 76, S58–S63. doi:10.1016/j.ijrobp.2009.06.090

Dietrich, M., Heselhaus, J., Wozniak, J., Weinandy, S., Mela, P., Tschoeke, B., et al. (2013). Fibrin-based Tissue Engineering: Comparison of Different Methods of Autologous Fibrinogen Isolation. *Tissue Eng. C: Methods* 19, 216–226. doi:10.1089/ten.tec.2011.0473

dos Santos, H. T., Kim, K., Okano, T., Camden, J. M., Weisman, G. A., Baker, O. J., et al. (2020). Cell Sheets Restore Secretory Function in Wounded Mouse Submandibular Glands. *Cells* 9, 2645. doi:10.3390/cells9122645

Dos Santos, H. T., Nam, K., Brown, C. T., Dean, S. M., Lewis, S., Pfeifer, C. S., et al. (2021). Trimers Conjugated to Fibrin Hydrogels Promote Salivary Gland Function. *J. Dent Res.* 100, 268–275. doi:10.1177/0022034520964784

Ferreira, J. N., Rungarunlert, S., Urkasemsin, G., Adine, C., and Souza, G. R. (2016). Three-Dimensional Bioprinting Nanotechnologies towards Clinical Application of Stem Cells and Their Secretome in Salivary Gland Regeneration. *Stem Cell Int.* 2016, 7564689. doi:10.1155/2016/7564689

Foraida, Z. I., Kamaldinov, T., Nelson, D. A., Larsen, M., and Castracane, J. (2017). Elastin-PLGA Hybrid Electrospun Nanofiber Scaffolds for Salivary Epithelial Cell Self-Organization and Polarization. *Acta Biomater.* 62, 116–127. doi:10.1016/j.actbio.2017.08.009

Frith, J. E., Mills, R. J., Hudson, J. E., and Cooper-White, J. J. (2012). Tailored Integrin-Extracellular Matrix Interactions to Direct Human Mesenchymal Stem Cell Differentiation. *Stem Cell Develop.* 21, 2442–2456. doi:10.1089/scd.2011.0615

Froelich, K., Pueschel, R. C., Birner, M., Kindermann, J., Hackenberg, S., Kleinsasser, N. H., et al. (2010). Optimization of Fibrinogen Isolation for Manufacturing Autologous Fibrin Glue for Use as Scaffold in Tissue Engineering. *Artif. Cell Blood Substitutes, Biotechnol.* 38, 143–149. doi:10.3109/10731191003680748

Grundmann, O., Fillinger, J. L., Victory, K. R., Burd, R., and Limesand, K. H. (2010). Restoration of Radiation Therapy-Induced Salivary Gland Dysfunction in Mice by post Therapy IGF-1 Administration. *BMC Cancer* 10, 417. doi:10.1186/1471-2407-10-417

Haderlein, M., Speer, S., Ott, O., Lettmaier, S., Hecht, M., Semrau, S., et al. (2020). Dose Reduction to the Swallowing Apparatus and the Salivary Glands by De-intensification of Postoperative Radiotherapy in Patients with Head and Neck Cancer: First (Treatment Planning) Results of the Prospective Multicenter DIREKHT Trial. *Cancers (Basel)* 12, doi:10.3390/cancers12030538

Hoffman, M. P., Nomizu, M., Roque, E., Lee, S., Jung, D. W., Yamada, Y., et al. (1998). Laminin-1 and Laminin-2 G-Domain Synthetic Peptides Bind Syndecan-1 and Are Involved in Acinar Formation of a Human Submandibular Gland Cell Line. *J. Biol. Chem.* 273, 28633–28641. doi:10.1074/jbc.273.44.28633

Hsiao, Y.-C., and Yang, T.-L. (2015). Data Supporting Chitosan Facilitates Structure Formation of the Salivary Gland by Regulating the Basement Membrane Components. *Data in brief* 4, 551–558. doi:10.1016/j.dib.2015.07.006

Huettner, N., Dargaville, T. R., and Forget, A. (2018). Discovering Cell-Adhesion Peptides in Tissue Engineering: Beyond RGD. *Trends Biotechnol.* 36, 372–383. doi:10.1016/j.tibtech.2018.01.008

Ikeda, E., Ogawa, M., Takeo, M., and Tsuji, T. (2019). Functional Ectodermal Organ Regeneration as the Next Generation of Organ Replacement Therapy. *Open Biol.* 9, 190010. doi:10.1098/rsob.190010

Jaguar, G. C., Prado, J. D., Campanhã, D., and Alves, F. A. (2017). Clinical Features and Preventive Therapies of Radiation-Induced Xerostomia in Head and Neck Cancer Patient: a Literature Review. *Appl. Cancer Res.* 37, 31. doi:10.1186/s41241-017-0037-5

Jasmer, K. J., Gilman, K. E., Muñoz Forti, K., Weisman, G. A., and Limesand, K. H. (2020). Radiation-Induced Salivary Gland Dysfunction: Mechanisms, Therapeutics and Future Directions. *J. Clin. Med.* 9, 4095. doi:10.3390/jcm9124095

Jensen, S. B., Vissink, A., Limesand, K. H., and Reyland, M. E. (2019). Salivary Gland Hypofunction and Xerostomia in Head and Neck Radiation Patients. *J. Natl. Cancer Inst. Monogr.* doi:10.1093/jncimonographs/lgz016

Jensen, S. B., au, fnm., Pedersen, A. M. L., Vissink, A., Andersen, E., Brown, C. G., et al. (2010). A Systematic Review of Salivary Gland Hypofunction and Xerostomia Induced by Cancer Therapies: Prevalence, Severity and Impact on Quality of Life. *Support Care Cancer* 18, 1039–1060. doi:10.1007/s00520-010-0827-8

Lombaert, I. M. A., Brunsting, J. F., Wierenga, P. K., Kampinga, H. H., de Haan, G., and Coppes, R. P. (2008). Keratinocyte Growth Factor Prevents Radiation Damage to Salivary Glands by Expansion of the Stem/Progenitor Pool. *Stem Cells* 26, 2595–2601. doi:10.1634/stemcells.2007-1034

Lovelace, T. L., Fox, N. F., Sood, A. J., Nguyen, S. A., and Day, T. A. (2014). Management of Radiotherapy-Induced Salivary Hypofunction and Consequent Xerostomia in Patients with Oral or Head and Neck Cancer: Meta-Analysis and Literature Review. *Oral Surg. Oral Med. Oral Pathol. Oral Radiol.* 117, 595–607. doi:10.1016/j.oooo.2014.01.229

Lung, C. B., Watson, G. E., Verma, S., Feng, C., and Saunders, R. H. (2021). Duration of Effect of Biotène spray in Patients with Symptomatic Dry Mouth: A Pilot Study. *Oral Surg. Oral Med. Oral Pathol. Oral Radiol.* 131, 415–421. doi:10.1016/j.oooo.2020.12.002

Mitroulia, A., Gavriiloglou, M., Athanasiadou, P., Bakopoulou, A., Poulopoulos, A., and Andreadis, D. (2019). Salivary Gland Stem Cells and Tissue Regeneration: An Update on Possible Therapeutic Application. *J. Contemp. Dent Pract.* 20, 978–986. doi:10.5005/jp-journals-10024-2620

Mochizuki, M., (2003). Current Awareness. *Hydrol. Process* 17, 875–877. doi:10.1002/hyp.5037

Motta, C. M. M., Endres, K. J., Wesdemiotis, C., Willits, R. K., and Becker, M. L. (2019). Enhancing Schwann Cell Migration Using Concentration Gradients of Laminin-Derived Peptides. *Biomaterials* 218, 119335. doi:10.1016/j.biomaterials.2019.119335

Nair, R. P., Zheng, C., and Sunavala-Dossabhoy, G. (2016). Retroductal Submandibular Gland Instillation and Localized Fractionated Irradiation in a Rat Model of Salivary Hypofunction. *JoVE*, 53785. doi:10.3791/53785

Nam, K., Dean, S. M., Brown, C. T., Smith, R. J., Lei, P., Andreadis, S. T., et al. (2019). Synergistic Effects of Laminin-1 Peptides, VEGF and FGF9 on Salivary Gland Regeneration. *Acta Biomater.* 91, 186–194. doi:10.1016/j.actbio.2019.04.049

Nam, K., Jones, J. P., Lei, P., Andreadis, S. T., and Baker, O. J. (2016). Laminin-111 Peptides Conjugated to Fibrin Hydrogels Promote Formation of Lumen Containing Parotid Gland Cell Clusters. *Biomacromolecules* 17, 2293–2301. doi:10.1021/acs.biomac.6b00588

Nam, K., Kim, K., Dean, S. M., Brown, C. T., Davis, R. S., Okano, T., et al. (2019). Using Cell Sheets to Regenerate Mouse Submandibular Glands. *NPJ Regen. Med.* 4, 16. doi:10.1038/s41536-019-0078-3

Nam, K., Maruyama, C. L., Wang, C.-S., Trump, B. G., Lei, P., Andreadis, S. T., et al. (2017). Laminin-111-derived Peptide Conjugated Fibrin Hydrogel Restores Salivary Gland Function. *PLoS One* 12, e0187069. doi:10.1371/journal.pone.0187069

Nam, K., Wang, C.-S., Maruyama, C. L. M., Lei, P., Andreadis, S. T., and Baker, O. J. (2017). L1 Peptide-Conjugated Fibrin Hydrogels Promote Salivary Gland Regeneration. *J. Dent Res.* 96, 798–806. doi:10.1177/0022034517695496

Nanduri, L. S. Y., Lombaert, I. M. A., van der Zwaag, M., Faber, H., Brunsting, J. F., van Os, R. P., et al. (2013). Salisphere Derived C-Kit+ Cell Transplantation Restores Tissue Homeostasis in Irradiated Salivary Gland. *Radiother. Oncol.* 108, 458–463. doi:10.1016/j.radonc.2013.05.020

Nanduri, L. S. Y., Maimets, M., Pringle, S. A., van der Zwaag, M., van Os, R. P., and Coppes, R. P. (2011). Regeneration of Irradiated Salivary Glands with Stem Cell Marker Expressing Cells. *Radiother. Oncol.* 99, 367–372. doi:10.1016/j.radonc.2011.05.085

Ogawa, M., Oshima, M., Imamura, A., Sekine, Y., Ishida, K., Yamashita, K., et al. (2013). Functional Salivary Gland Regeneration by Transplantation of a Bioengineered Organ Germ. *Nat. Commun.* 4, 2498. doi:10.1038/ncomms3498

Ogawa, M., and Tsuji, T. (2015). Reconstitution of a Bioengineered Salivary Gland Using a Three-Dimensional Cell Manipulation Method. *Curr. Protoc. Cel Biol.* 66, 19. doi:10.1002/0471143030.cb1917s66

Patil, S. V., and Nanduri, L. S. Y. (2017). Interaction of Chitin/chitosan with Salivary and Other Epithelial Cells-An Overview. *Int. J. Biol. Macromolecules* 104, 1398–1406. doi:10.1016/j.ijbiomac.2017.03.058

Peters, S. B., Naim, N., Nelson, D. A., Mosier, A. P., Cady, N. C., and Larsen, M. (2014). Biocompatible Tissue Scaffold Compliance Promotes Salivary Gland Morphogenesis and Differentiation. *Tissue Eng. Part A* 20, 1632–1642. doi:10.1089/ten.tea.2013.0515

Pinna, R., Campus, G., Cumbo, E., Mura, I., and Milia, E. (2015). Xerostomia Induced by Radiotherapy: an Overview of the Physiopathology, Clinical Evidence, And management of the Oral Damage. *Tcrm* 11, 171–188. doi:10.2147/tcrm.s70652

Pradhan-Bhatt, S., (2014). A Novel *In Vivo* Model for Evaluating Functional Restoration of a Tissue-engineered Salivary Gland. *Laryngoscope* 124, 456–461. doi:10.1002/lary.24297

Pringle, S., Van Os, R., and Coppes, R. P. (2013). Concise Review: Adult Salivary Gland Stem Cells and a Potential Therapy for Xerostomia. *Stem Cells* 31, 613–619. doi:10.1002/stem.1327

Rebustini, I. T., Patel, V. N., Stewart, J. S., Layvey, A., Georges-Labouesse, E., Miner, J. H., et al. (2007). Laminin α5 Is Necessary for Submandibular Gland Epithelial Morphogenesis and Influences FGFR Expression through β1 Integrin Signaling. *Develop. Biol.* 308, 15–29. doi:10.1016/j.ydbio.2007.04.031

Rocchi, C., and Emmerson, E. (2020). Mouth-Watering Results: Clinical Need, Current Approaches, and Future Directions for Salivary Gland Regeneration. *Trends Mol. Med.* 26, 649–669. doi:10.1016/j.molmed.2020.03.009

Siegel, R. L., Miller, K. D., Fuchs, H. E., and Jemal, A. (2021). Cancer Statistics, 2021. *CA A. Cancer J. Clin.* 71, 7–33. doi:10.3322/caac.21654

Silvestre, F. J., Minguez, M. P., and Suñe-Negre, J. M. (2009). Clinical Evaluation of a New Artificial Saliva in spray Form for Patients with Dry Mouth. *Med. Oral Patol Oral Cir Bucal* 14, E8–E11.

Soscia, D. A., Sequeira, S. J., Schramm, R. A., Jayarathanam, K., Cantara, S. I., Larsen, M., et al. (2013). Salivary Gland Cell Differentiation and Organization on Micropatterned PLGA Nanofiber Craters. *Biomaterials* 34, 6773–6784. doi:10.1016/j.biomaterials.2013.05.061

Sroussi, H. Y., Epstein, J. B., Bensadoun, R.-J., Saunders, D. P., Lalla, R. V., Migliorati, C. A., et al. (2017). Common Oral Complications of Head and Neck Cancer Radiation Therapy: Mucositis, Infections, Saliva Change, Fibrosis, Sensory Dysfunctions, Dental Caries, Periodontal Disease, and Osteoradionecrosis. *Cancer Med.* 6, 2918–2931. doi:10.1002/cam4.1221

Su, X., Liu, Y., Bakkar, M., ElKashty, O., El-Hakim, M., Seuntjens, J., et al. (2020). Labial Stem Cell Extract Mitigates Injury to Irradiated Salivary Glands. *J. Dent Res.* 99, 293–301. doi:10.1177/0022034519898138

Sun, T., Zhu, J., Yang, X., and Wang, S. (2006). Growth of Miniature Pig Parotid Cells on Biomaterials *In Vitro*. *Arch. Oral Biol.* 51, 351–358. doi:10.1016/j.archoralbio.2005.10.001

Turner, M. D. (2016). Hyposalivation and Xerostomia. *Dental Clin. North America* 60, 435–443. doi:10.1016/j.cden.2015.11.003

Varghese, J. J., Schmale, I. L., Mickelsen, D., Hansen, M. E., Newlands, S. D., Benoit, D. S. W., et al. (2018). Localized Delivery of Amifostine Enhances Salivary Gland Radioprotection. *J. Dent Res.* 97, 1252–1259. doi:10.1177/0022034518767408

Weng, P.-L., Aure, M. H., Maruyama, T., and Ovitt, C. E. (2018). Limited Regeneration of Adult Salivary Glands after Severe Injury Involves Cellular Plasticity. *Cel Rep.* 24, 1464–1470. doi:10.1016/j.celrep.2018.07.016

Wu, V. W. C., and Leung, K. Y. (2019). A Review on the Assessment of Radiation Induced Salivary Gland Damage after Radiotherapy. *Front. Oncol.* 9, 1090. doi:10.3389/fonc.2019.01090

Yang, T.-L., and Hsiao, Y.-C. (2015). Chitosan Facilitates Structure Formation of the Salivary Gland by Regulating the Basement Membrane Components. *Biomaterials* 66, 29–40. doi:10.1016/j.biomaterials.2015.06.028

Zheng, C., Cotrim, A. P., Rowzee, A., Swaim, W., Sowers, A., Mitchell, J. B., et al. (2011). Prevention of Radiation-Induced Salivary Hypofunction Following hKGF Gene Delivery to Murine Submandibular Glands. *Clin. Cancer Res.* 17, 2842–2851. doi:10.1158/1078-0432.ccr-10-2982

Conflict of Interest: The authors declare that the research was conducted in the absence of any commercial or financial relationships that could be construed as a potential conflict of interest.

Publisher's Note: All claims expressed in this article are solely those of the authors and do not necessarily represent those of their affiliated organizations, or those of the publisher, the editors and the reviewers. Any product that may be evaluated in this article, or claim that may be made by its manufacturer, is not guaranteed or endorsed by the publisher.